Articles

A Three-Dimensional Model of Lanosterol 14α-Demethylase of *Candida albicans* and Its Interaction with Azole Antifungals

Haitao Ji,* Wannian Zhang,* Youjun Zhou, Min Zhang, Jie Zhu, Yunlong Song, Jiaguo Lü, and Jü Zhu

School of Pharmacy, Second Military Medical University, 325 Guohe Road, Shanghai 200433, People's Republic of China

Received November 30, 1999

The three-dimensional structure of lanosterol 14α-demethylase ($P450_{14DM}$, CYP51) of *Candida albicans* was modeled on the basis of crystallographic coordinates of four prokaryotic P450s: P450BM3, P450cam, P450terp, and P450eryF. The $P450_{14DM}$ sequence was aligned to those of known proteins using a knowledge-based alignment method. The main chain coordinates of the core regions were transferred directly from the corresponding coordinates of P450BM3. The side chain conformations of the core regions were determined by the conformations of the equivalent residues with the highest homologous scores in four crystal structures. The model was then refined using molecular mechanics and molecular dynamics. The reliability of the resulting model was assessed by Ramachandran plots, Profile-3D, hydropathy plot analysis, and by analyzing the consistency of the model with the experimental data. The structurally and functionally important residues such as the heme binding residues, the residues interacting with redox-partner protein and/or involved in electron transfer, the residues lining substrate access channel, and the substrate binding residues were identified from the model. These residues are candidates for further site-directed mutagenesis and site-specific antipeptide antibody binding experiments. The active analogue approach was employed to search the pharmacophoric conformations for 14 azole antifungals. The resulting bioactive conformations were docked into the active site of lanosterol 14α-demethylase of *Candida albicans*. All 14 azole antifungals are shown to have a similar docking mode in the active site. The halogenated phenyl group of azole inhibitors is deep in the same hydrophobic binding cleft as the 17-alkyl chain of substrate. The $\pi-\pi$ stacking interaction might exist between halogenated phenyl ring of inhibitors and the aromatic ring of residue Y132. The long side chains of some inhibitors such as itraconazole and ketoconazole surpass the active site and interact with the residues in the substrate access channel. To compare with mammalian enzymes, structurally selective residues of the active site of fungal lanosterol 14α-demethylase are distributed in the C terminus of F helix, β6-1 sheet and β6-2 sheet.

Introduction

Lanosterol 14α-demethylase ($P450_{14DM}$, CYP51) is a member of the cytochrome P450 superfamily, which catalyzes the removal of the 14-methyl group (C-32) of lanosterol via three successive monooxygenation reactions. The first two of these reactions are conventional cytochrome P450 hydroxylations that produce the 14-hydroxymethyl and 14-carboxyaldehyde derivatives of lanosterol.[1,2] In the final step, the 14-aldehyde group is eliminated as formic acid with concomitant introduction of a $\Delta^{14,15}$ double bond.[3−5] $P450_{14DM}$ occurs in different kingdoms, such as fungi, higher plants, and animals, with the same metabolic role, i.e., removal of the 14-methyl group of sterol precursors such as lanosterol, obtusifoliol, dihydrolanosterol, and 24(28)-methylene-24,25-dihydrolanosterol,[6] and this is the only known P450 distributed widely in eukaryotes with essentially the same metabolic role.[7,8]

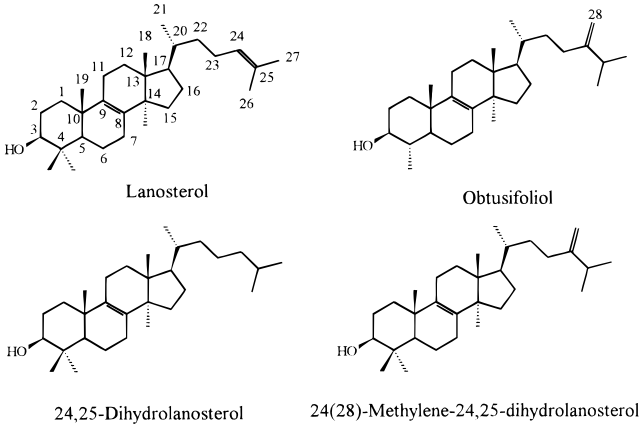

In yeasts and fungi, $P450_{14DM}$ participates in ergosterol biosynthesis and is an essential requirement for fungal viability.[9] Selective inhibition of the enzyme would cause depletion of ergosterol and accumulation of lanosterol and some other 14-methyl sterols and result in the growth inhibition of fungal cell. The inhibitors include imidazole and triazole antifungal

* To whom inquiries should be addressed. For W.Z.: Phone: 86-21-25070321. Fax: 86-21-65490641. E-mail: Zhangwnk@online.sh.cn. For H.J.: Phone: 86-21-25070354. E-mail jihaitao@online.sh.cn.

10.1021/jm990589g CCC: $19.00
Published on Web 06/10/2000

agents such as ketoconazole and fluconazole, which are well-established drugs for the treatment of topical and systemic mycoses.

Although the amino acid sequences of $P450_{14DM}$ from higher plants,[10] bacteria,[11] fungi,[12,13] and mammals[14,15] have been characterized and substrate specificity and inhibitor selectivity of $P450_{14DM}$ have been investigated by the indirect methods, structure−function analysis has not been rigorously approached. There are, for example, no site-directed mutagenesis data that would pinpoint key substrate and/or inhibitors binding residues, the heme binding residues, and the residues interacting with redox-partner protein and/or involved in electron transfer. Due to the importance of $P450_{14DM}$ in antifungal drugs study, it is of great interest to understand how this enzyme functions, in particular the nature and structural requirements of its substrate and inhibitor binding sites. These studies will be facilitated by information about the three-dimensional (3D) structure, which would allow a detailed analysis of enzyme−substrate and enzyme−inhibitor interactions and help the rational design of new antifungal agents. Experimental methods, such as X-ray crystallography or multiple dimensional NMR, are being used to obtain 3D structures of proteins and protein−ligand complexes. However, these techniques are difficult to apply to large membrane proteins such as $P450_{14DM}$. The only X-ray coordinates of cytochrome P450 available are not membrane-bound and belong to prokaryotic microorganisms: P450cam from *Pseudomonas putida*,[16] P450terp from *Pseudomonas sp*,[17] P450eryF from *Saccaropolyspora erythrea*,[18] and P450BM3 from *Bacillus megaterium*.[19] Among them, P450cam, P450terp, and P450eryF are the class I cytochrome P450s that receive their NADH-derived electrons from a two-protein redox chain (FAD redutase → iron-sulfur protein → P450). P450BM3 is a class II cytochrome P450 that receives NADPH-derived electrons directly from an FAD/FMN-containing reductase in a similar manner as microsomal cytochrome P450s do.

Although pairwise sequence identities of the four prokaryotic P450s are generally low (19−26%), their topology is quite similar. Most of the secondary and supersecondary structural motifs, characteristically hydrophobic and hydrophilic segments, and the regions of the sequence containing the heme binding site, the oxygen binding site, and the site of interactions with redox partners are highly conserved. A 3D superposition of the P450s mentioned above permits the definition of spatially conserved regions (SCRs), which include the heme-binding core region, especially the bottom and the side of the substrate binding pocket.[20,21] On the other hand, site-directed mutagenesis, antibody recognition information, and photoaffinity labeling have found that many functional residues and segments were conserved. These findings provided the rationale for a reliable 3D modeling of mammalian P450s despite their low degree of homology with prokaryotic P450s.

On the basis of the premise of structural homology among cytochrome P450s, molecular models of various microsomal P450s have been constructed. The initial models, based on the structure of P450cam, the only known P450 structure at that time, included CYP1A1,[22] CYP2B1,[23] CYP17,[24] CYP19A1,[25] CYP21.[24] More recent models were based on the structure of P450BM3 due to their structural and functional similarity, for example, the models of CYP1A2,[26,27] CYP2A6,[28] CYP2B1,[29,31] CYP3A4,[26] CYP5[33], CYP17,[30] CYP19[30,32] and CYP21.[30] In the case of CYP51 from *Candida albicans*, only the 3D structures were modeled on the basis of the crystallographic coordinates of P450cam and P450eryF by Boscott,[34] Tsukuda,[35] and Höltje,[36] respectively.

When the degree of homology between the studied protein and the available 3D templates is low, as occurs in members of the cytochrome P450 superfamily, model building becomes a difficult task and the reliability of the results depends critically on the correctness of the sequence alignment. In this case, the accuracy of the alignment may be improved by taking into account further structural information. That is, the method of knowledge-based sequence alignment is more suitable than the automatic multiple alignment procedure utilized in the previous 3D structure modeling of $P450_{14DM}$.

Therefore, in the present investigation, we constructed a model of P45014DM from *Candida albicans*, which was built on the basis of the four known crystal structures, P450cam, P450terp, P450eryF, and P450BM3. The sequence of P45014DM was aligned to those of known proteins using a knowledge-based alignment method. Such a model should include structural information from all known enzymes and lead to a more accurate model structure. The model can be used to explain substrate specificity and relate enzyme function to its structure. For this purpose, the docking of substrate and some azole antifungals into the active site of the model was explored. The structurally and functionally important residues identified allowed for a better understanding of the structure−function relationships of the enzyme. The modes of the enzyme−substrate and enzyme−inhibitor interactions would be useful in developing more potent antifungal drugs.

Materials and Methods

General. The crystallographic coordinates of P450cam (1.63 Å resolution, $R_{cryst} = 0.19$), P450terp (2.3 Å resolution, $R_{cryst} = 0.19$), P450eryF (2.1 Å resolution, $R_{cryst} = 0.19$), and P450BM3 (2.0 Å resolution, $R_{cryst} = 0.17$) were obtained from the Brookhaven Protein Databank as entries 2CPP, 1CPT, 1OXA, and 2HPD. The sequences of $P450_{14DM}$ were from PIR database. Molecular modeling was performed with the commercially available SYBYL6.2 software package[37] and MSI Insight II 98 software package.[38] All calculations were performed on a Silicon Graphics Iris Indigo II XZ workstation.

Sequence Alignment. To align the seqences of $P450_{14DM}$ to those of P450cam, P450terp, P450eryF, and P450BM3, we utilized the knowledge-based alignment, which was a modification of structure-based alignment proposed by Hasemann et al.[21,22] Four crystal structures were superimposed by root-mean-square (rms) fit of the porphyrin ring carbon atoms of the prosthetic group heme to obtain the structure-based sequence alignment. The SCRs of the four proteins were determined on the basis of rms deviations of the backbone for each pair of structures. The sequence of $P450_{14DM}$ was aligned to that of P450BM3 using the Needleman−Wunsch algorithm.[39] The pmutation homology matrix was used for evaluating amino acid similarity. The number of gap penalty and jumbles were 8 and 10, respectively. The alignment was then manually optimized on the basis of a variety of goals: (1) To match known secondary elements in the four crystal structures to those predicted for $P450_{14DM}$ by Bayes statistics.[40] (2) To locate insertions and deletions in $P450_{14DM}$ relative to known proteins outside predicted α-helical and β-sheet regions. (3)

```
Cam                                          --NLAPLPPHVPEHLV--F-DF--DMYNPSNLSAGVQEAWAVLQES--NVPDLV 54
Terp                                         ------MDARAT--IPEHIARTVILPQGYA-----DDEVIYPAFKWLRDEQPLA 41
eryF                                         -------------ATV--P-DL--ESDSF------HVD-WYSTYAELRETAPVT 30
BM3                                          TIKEMPQPKTFGELKNLPLLN-----TD------KPVQALMKIADELG---EIF 40
C.A. MAIVETVIDGINYFLSLSVTQQISILLGVPFVYNLVWQYLYSLRKDRAPLVFYWIPWFGSAAS----YGQ-----QPYEFFESCRQKYG---DVF 83
                                 T-M                          A'                          A

cam  WTRCNG--GHWIATRGQLIREAYEDYRHFSSE------CP-FI-PREAGEAY----------DPIPTSMDPP--EQRQFRALANQVVGMPVVDKL 127
terp MAHIEGYDPMWIATKHADVMQIGKQPGLFSNAEG----SE-ILYDQNNEAFMRSISGGCPHVIDSLTSMDPP--THTAYRGLTLNWFQPASIRKL 129
eryF PVRFLG-QDAWLVTGYDEAKAALSDL-RLSSDPKKKYPGVEVEFPAYLGFPEDVRNYF----ATNMGTSDPP--THTRLRKLVSQEFTVRRVEAM 117
BM3  KFEAPG-RVTRYLSSQRLIKEACDES-RFDKN------LS----QALKFVRDFAG-------DGLFTSW-THEKNWKKAHNILLPSFSQQAMKGY 115
C.A. SFMLLGKIMTVYLGPKGHEFVFNAKLSDVSAE-----DAYK---HLTTPVFGKGV-------IYDCPNS-RLMEQKKFAKFALTTDSFKRYVPKI 162
     1-1      1-2     B          1-5                  B'              Meander1     C              C*

cam  ENRIQELACSLIESLRPQ---GQCNFTEDYAEPFPIRIFMLLAG-LPEED-----IPHLKYLTDQMTR---PDGSM---------TFAEAKEALY 199
terp EENIRRIAQASVQRLLDF--DGECDFMTDCALYYPLHVVMTALG-VPEDD-----EPLMLKLTQDFFGVHEPDEQAVAAPRQSADEAARRFHETI 216
eryF RPRVEQITAELLDEVGDS---GVVDIVDRFAHPLPIKVICELLG-VDEAA-----RGAFGRWSSEILVM---DP-------ERAERQGQAAREVV 193
BM3  HAMMVDIAVQLVQKWERLNADEHIEVPE-DMTRLTLDTIGLCGFNYRFNSFYRDQPHPFITSMVRALDEAMNKLQRANPDDPAYDENKRQFQEDI 209
C.A. REEILNYFVTDESFKLKEKTHGVANVMK-TQPEITIFTASRSLF-GDEMRRIF---DRSFAQLYSDLDKGFTPINFVFPNLPLPHYWRRDAAQKK 252
          D                 3-1   E*        E                          F                              G

cam  DYLIPIIEQRRQKP-----GT-DAISIVANGQV--NGRPITSDEAKRMCGLLLVGGLDTVVNFLSFSMEFLAKSPEHRQELIERP---------- 278
terp ATFYDYFNGFTVDRRSC-P-KDDVMSLLANSKL--DGNYIDDKYINAYYVAIATAGHDTTSSSSGGAIIGLSRNPEQLALAKSDP---------- 297
eryF NFILDLVERRRTEP-----GD-DLLSALISVQDD-DDGRLSADELTSIALVLLLAGFEASVSLIGIGTYLLLTHPDQLALVRADP---------- 271
BM3  KVMNDLVDKIIADRKASGEQSDDLLTHMLNGKDPETGEPLDDENIRYQIITFLIAGHETTSGLLSFALYFLVKNPHVLQKAAEEAARVLVDPVP- 303
C.A. ISATYMKEIKLRRERGDIDPNRDLIDSLLIHSTYKDGVKMTDQEIANLLIGILMGGQHTSASTSAWFLLHLGEKPHLQDVIYQEVVELLKEKGGD 347
                            H    5-1     5-2                  I                          J

cam  ------------ERIPAACEELLRRFSLV-ADGRILTSDYEFHG--VQLKKGDQILLPQMLSGLDERENA-CPMHVDFSR--QK---------- 344
terp ------------ALIPRLVDEAVRWTAPVKSFMRTALADTEVRG--QNIKRGDRIMLSYPSANRDEEVFS-NPDEFDITRF--P---------- 364
eryF ------------SALPNAVEEILRYIAPPETTTRFAAEEVEIGG--VAIPQYSTVLVANGAANRDPSQFP-DPHRFDVTR---D---------- 337
BM3  ----SYKQVKQLKYVGMVLNEALRLWPTAPAFSLYAKEDTVLGG-EYPLEKGDELMVLIPQLHRDKTIWGDDVEEFRPERFENPSA--------- 384
C.A. LNDLTYEDLQKLPSVNNTIKETLRMHMPLHSIFRKVTNPLRIPETNYIVPKGHYVLVSPGYAHTSERYFDNPEDFDPTRWDTAAAKANSVSFNSS 442
          J'         K        6-1  1-4     2-1     2-2     1-3     K'     K''    Meander

cam  ------------VS---HTTFGHGSHLCLGQHLARREIIVTLKEWLTRIPDFSIAPGA---Q-IQHKS-GIVSGVQALPLVWDPATTKAV- 414
terp ------------NR---HLGFGWGAHMCLGQHLAKLEMKIFFEELLPKL-KSVE-L-S---GDPRLYATNFVGGPKNVPIRFTKA------ 428
eryF ------------TR--GHLSFGQGIHFCMGRPLAKLEGEVALRALFGRFPALSLG--IDADD-VVWRRSLLLRGIDHLPVRLDG------- 404
BM3  ------------IPQHAFKPFGNGQRACIGQQFALHEATLVLGMMLKHF-DFEDH-TN-Y--ELDIKE-TLTLKPEGFVVKAKSKKIPLGG 457
C.A. DEVDYGFGKVSKGVSSPYLPFGGGRHRCIGEQFAYVQLGTILTTFVYNL-RWTID-GYKV-PDPDYSS-MVVLPTEPAEIIWEKRETCMF- 528
                        Cys-pocket        L                 3-3          4-1  6-2 4-2    3-2
```

Figure 1. Sequence alignment between P450 51 from *C. albicans*, P450BM3, P450terp, and P450eryF. α-Helices and *β*-sheets are underlined and named using the same convention as that used for P450BM3 and P450terp.[20] T−M means the trans-membrane region. The position number of the amino acid sequence is shown at the far right of each line. The core regions are showned in bold.

To match structurally and functionally important irregular SCRs such as the Cys-pocket, Meander, and Meander1 identified from the crystal structure comparisons. (4) To align key conserved structural residues, for example, the axial heme cysteinyl ligand and residues involved in catalysis, ion pairing, and electron transfer. (5) To match characteristically hydrophobic and hydrophilic segments identified by hydropathy plot analysis with the parameters of Kyte−Doolittle and a window size of 9.[41] The final alignment spanned residues S42−F528 of $P450_{14DM}$ (Figure 1). The first 41 residues were assumed to comprise the membrane-binding region, and so had no counterparts in the four known proteins.

3D Model Building. The above alignment result identified 15 core regions where $P450_{14DM}$ and P450BM3 aligned, linked by 16 loops. Main chain coordinates of the core regions were transferred directly from the corresponding coordinates of P450BM3. Side chain conformations of the core regions were determined by the conformations of the equivalent residues with the highest homologous scores in the four crystal structures. Coordinates for the remaining residues in the loops were obtained using a fragment-searching approach.[42] If any homologue of the four known template structures had a loop of the same length in the corresponding region as the model, this fragment was selected. If no such compatible segment existed in the homologues, the loop was extracted from the PDB database and 10 best candidate structures were provided according to the minimum rms deviation of the Cα trace between the residues adjacent to the fragment considered (five adjacent residues per side). The best loop was then selected on the basis of the analysis result of the Profile-3D program,[43] which measured the compatibility between the protein sequence profile and its 3D profile.

The resulting model was subjected to a energy minimization using the following parameters: a distance-dependent dielectric constant, nonbonded cutoff of 8 Å, AMBER force field (Kollman all atoms parameters), and steepest descent minimization, until an energy gradient tolerance of 1kcal/mol Å was satisfied. Energy minimization was started with the loop side chains, the least well-defined parts of the structure, and gradually introduced those parts of the structure that could be expected to be predicted with greater certainty. That is, the undetermined core side chains, then the loop main chains, all the core side chains, and finally the core main chains. Heme extracted from the X-ray structure of P450BM3 was added to the $P450_{14DM}$ model, and residues neighboring heme were minimized as described above. The parameters for heme and ferryl oxygen were the same as described by Paulsen and Ornstein.[44] Finally, a conjugate gradient of the full proteins was performed until the rms gradient energy was lower than 0.1 kcal/mol Å. During the optimization procedure, the structure was checked periodically by Profile-3D and Ramachandran plots.

Docking the Substrate into the Active Site. The intrinsic substrate of $P450_{14DM}$ from *C. albicans*, 24(28)-methylene-24,25-dihydrolanosterol was built from the SYBYL fragment library. Energy minimization was performed using the Tripos force field, Powell optimization method, and MAXIMIN2 minimizer with a convergence criterion of 0.001 kcal/mol Å. Charges were calculated by the Gasteiger−Hückel method. Simulated annealing was then performed. The system was heated at 1000 K for 1.0 ps and then annealed to 250 K for 1.5 ps. The annealing function was exponential; 50 such cycles of annealing were run and the resulting 50 conformers were optimized using the methods described above. The lowest energy conformation was selected. The partial atomic charges of the resulting molecule were calculated with the AM1 method of MOPAC 6.0.

The substrate was placed in a reactive binding orientation with the oxidative site fixed at 4.2−5.5 Å from the heme iron. The C32−H bond aligned with the ferryl oxygen, heme iron and sulfur of C470. This resulted in a hydrogen-bonding distance between the ferryl oxygen and the hydrogen atom to be abstracted from the substrate. The nonbond interaction energy between the sterol and the protein, both electrostatic and van der Waals forces, was evaluated with SYBYL/Interactive docking to find the low-energy binding orientations. To the optimize enzyme−substrate interaction, the substrate was fixed in a low-energy binding orientation, and the residues in contact with the substrate (less than 4 Å distance) were minimized using the steepest descent method until the gradient was less than 1 kcal/mol Å. A molecular dynamics simulated annealing procedure was applied to the loop, the substrate binding residues within 4 Å from the substrate. The system was heated at 700 K for 10 ps, and then annealed to 200 K for 10 ps. During the substrate docking and energy optimization, the structure was checked periodically by Profile-3D and Ramachandran plots.

Docking of the Inhibitors into the Active Site. The azole antifungals in Figure 2 were built from X-ray coordinates when they were available or from the SYBYL fragment library. All the molecules were drugs or candidates for clinical and preclinical trials. The global minimum energy conformations were explored by the same simulated annealing procedure as that of the substrate described above.

The active analogue approach was employed to search for the pharmacophoric conformations of Cmp7−Cmp14. Four pharmacophores had been identified by the extensive SAR analyses (Figure 3A): (1) N4(3) of the azole ring,[45,46] (2) the centroid of the phenyl ring,[45,47,48] (3) the oxygen atom attached to C2[47,49,50], and (4) the methyl group attached to C3.[49,51] The distances between pharmacophores (D1−D4) of those more rigid molecules were used as a constraint to reduce the number of conformations for the following molecules by using the SYBYL systematic search/distance map. Torsional angles $\tau 1-\tau 6$ were regarded as the rotatable bonds and searched over 0°−359° ranges. All rotatable bonds were varied systematically in 10° increments. The general van der Waals scaling factors were 1.00 (general), 0.87 (one-four interaction), and 0.65 (hydrogen bonding). The grid size for distance map constraints was 0.2 Å. After filter, conformers of each molecule were then subjected to an energy minimization. The first minimized conformer was stored in a molecular database directly. The following conformers were compared with the stored conformers sequentially in term of a rms fit of four pharmacophores, considering conformations with rms deviation below 0.03 as being identical. In the case of identical conformations, the conformation with the lowest energy was kept. The distances between pharmacophores were measured again to exclude those conformations dissatisfying the distance constraints due to energy minimization. Then, the resulting conformation with the lowest energy was chosen as the bioactive conformation. The conformation spaces of Cmp1−Cmp6 were sampled by a systematic search method and the distances D1−D3 in Figure 3B were constrained. Lowest energy conformations were also chosen as the bioactive conformations. The partial atomic charges of the bioactive conformation were calculated with the AM1 method of MOPAC 6.0.

Azole antifungals inhibited the binding of substrate to $P450_{14DM}$ by coordination of N4(3) of their azole rings to the sixth coordination position of the iron atom of the heme. So the bioactive conformations of azoles were placed into the active site with N4(3) of the azole ring fixed at 2.043 Å from the heme iron, i.e., the same as the crystal structure of P450cam complex with the azole inhibitors.[52] N4(3) was aligned with the heme iron and the sulfur of C470. The Fe−N bond was regarded as the rotatable bond and a 5° increment was used. Then, 72 spatial orientations of azole antifungals in the active site were evaluated with SYBYL/Interactive docking to find the one with lowest binding energy. To optimize enzyme−inhibitor interactions, inhibitor was fixed in a low-energy binding orientation, and residues in contact with the inhibitor (within 6 Å) were minimized using the steepest descent method until the gradient was less than 1 kcal/mol Å. The system was then minimized using conjugate gradients to a maximum gradient of 0.1 kcal/mol Å.

Results and Discussion

Modeling of $P450_{14DM}$ and General Features of the Model. The model of P45014DM from *C. albicans* in complex with its substrate was predicted on the basis of the sequence alignment and the four crystal structures, as presented in Figure 4. For comparison with the template, the 3D model of $P450_{14DM}$ was superimposed onto the X-ray structure of the P450BM3. The rms deviations were 0.4944 Å for the backbone and 0.9145 Å for all the atoms. The largest deviations occurred in the helices A, B′, and G; the F−G loop; β-sheet 2; and the N-terminal loop of the model. On the other hand, as would be expected, regions of the structures such as helices E, I, J, K, and L; Cys-pocket; Meander; Meander1; and β-sheet 6, which were closely similar in the crystal structures, were well-defined in our model. There were two major insertions in the $P450_{14DM}$ model from residues D347 to L351 (between helices J and J′), and from residues A434 to K454 (between Meander and the Cys-pocket). These insertions formed extended turn structures in the surface of the model. Nine smaller insertions and three deletions, with one to three residues each, were located in $P450_{14DM}$ residues S63, Q66, K90, S110, D116, K119, T392, K499, and P501 for insertions and in P450BM3 residues N163, D168−P170, and G457 for deletions. Most of the insertions and deletions exposed on the molecular surface did not cause large perturbations in the protein backbone folding or the structural core relative to those in P450BM3. We had little confidence in modeling M1−Y41 because of the absence of structural information for these residues. However, the sequence from Q22 to L40 was predicted to be a strongly hydrophobic helix. This segment showed the classical feature of a membrane-spanning region, a long run of primarily hydrophobic amino acids followed by several polar or charged residues.

To evaluate the quality of the modeled structure, both Ramachandran plots and Profile-3D were used for analysis. After molecular dynamics, 85.0% of the residues were in the most favored regions, 10.1% were in additional allowed region, 4.1% were in generously allowed region, and 0.8% were in disallowed region. Thus, a total of 95.1% of residues of the modeled structure after molecular dynamics was in the allowed region, which indicated that the backbone dihedral angles Φ and Ψ in the model were reasonable. In

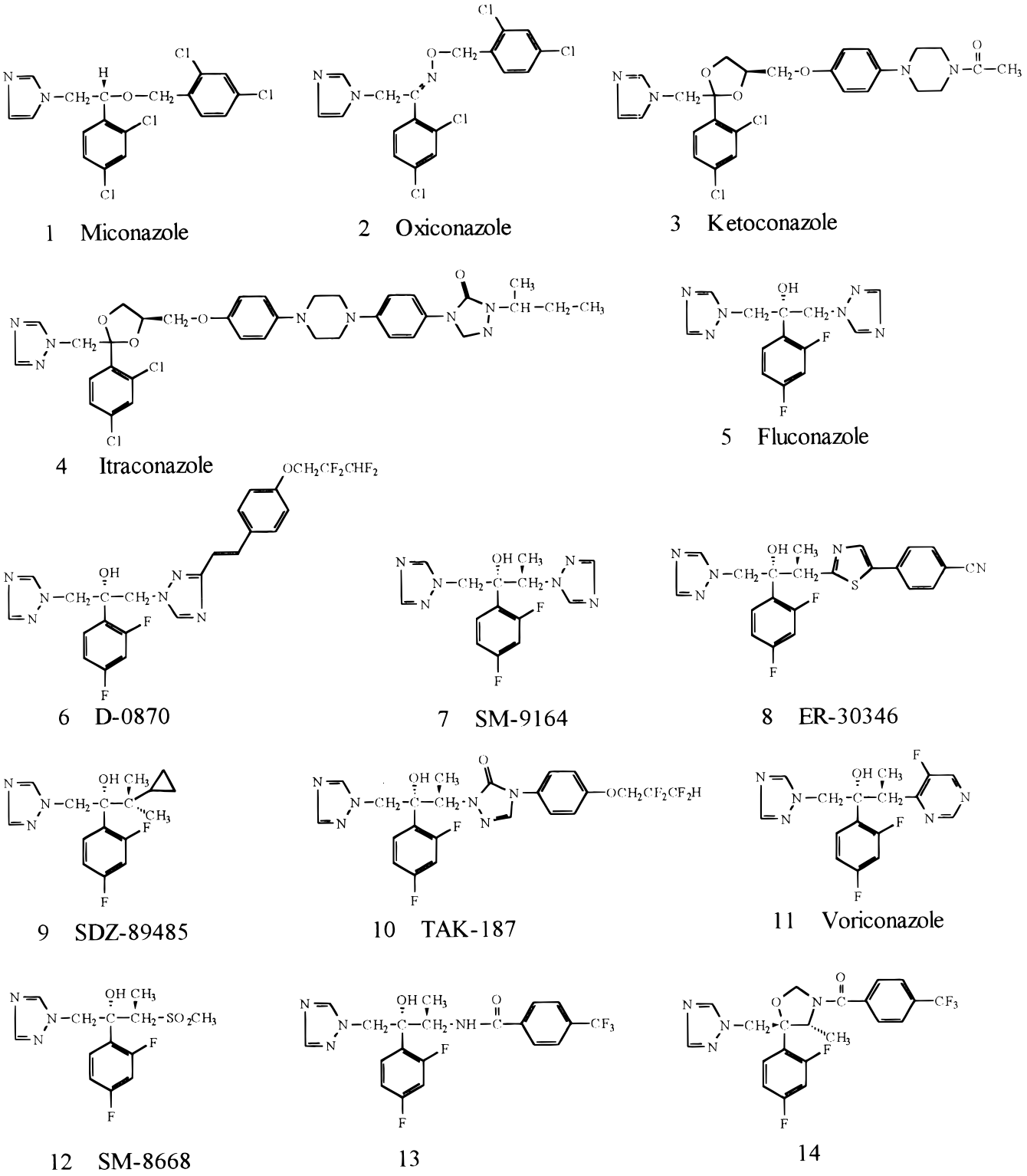

Figure 2. Structures of azole antifungals used in conformation analysis.

Profile-3D, the individual residues were characterized by their environment as determined from the area of buried residues, the fraction of side chain area that was covered by polar atoms, and the local secondary structure. The 3D profile score S for the compatibility of the sequence with the $P450_{14DM}$ model was within the limits of an acceptable value ($S > 0$), similar to that found for P450BM3. The distribution of the hydrophobic and hydrophilic segments was also similar to that of the crystal structures, which was typical of a globular protein. The hydrophilic segments including helix A, β1-5—N-terminal of helix B′, N-terminus of helix C, N-terminus and C-terminus of helix D, N-terminus of helix F, N-terminus and C-terminus of helix G, β5, helix J′, and helix K″—Meander pointed out into the cytoplasm environment. Helices E, I, and L were the characteristically hydrophobic segments. Especially helix I consisted of 34 amino acid residues with a distortion at the center

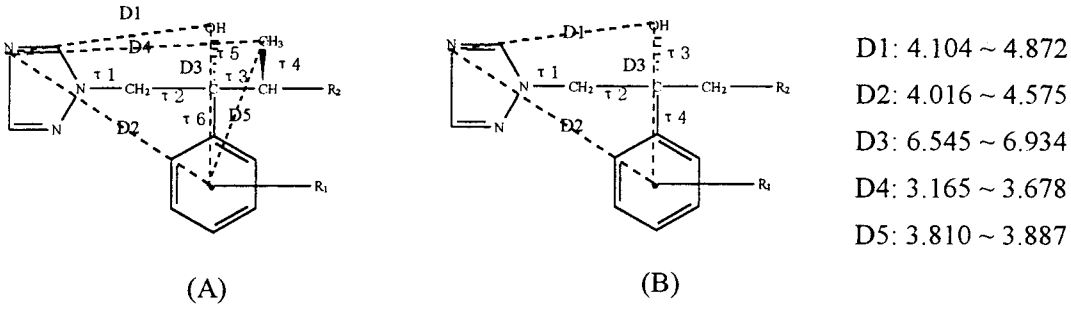

Figure 3. Proposed pharmacophore model, rotated bonds, distance mapping patterns, and results of distance mapping (D1−D5, Å) for azole antifungals.

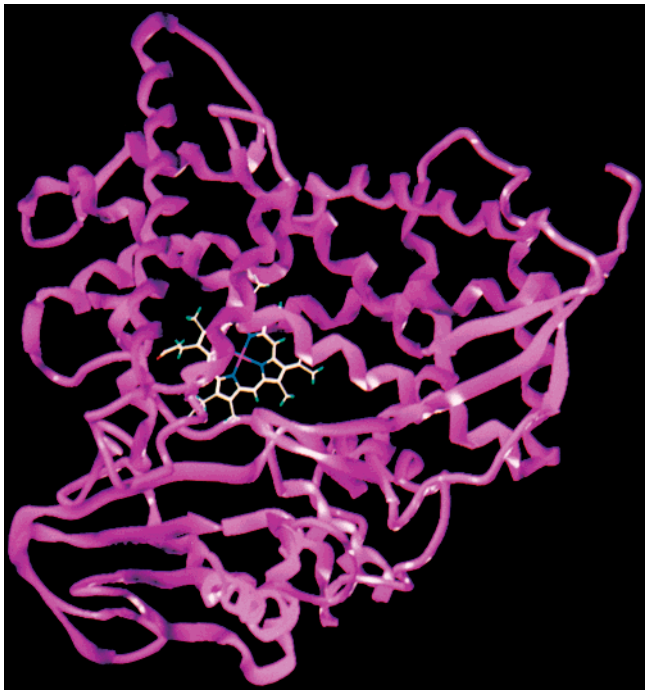

Figure 4. Ribbon representation of $P450_{14DM}$ model of *C. albicans*. The molecule is viewed from the substrate access (distal) face. Heme and substrate are also shown in the model.

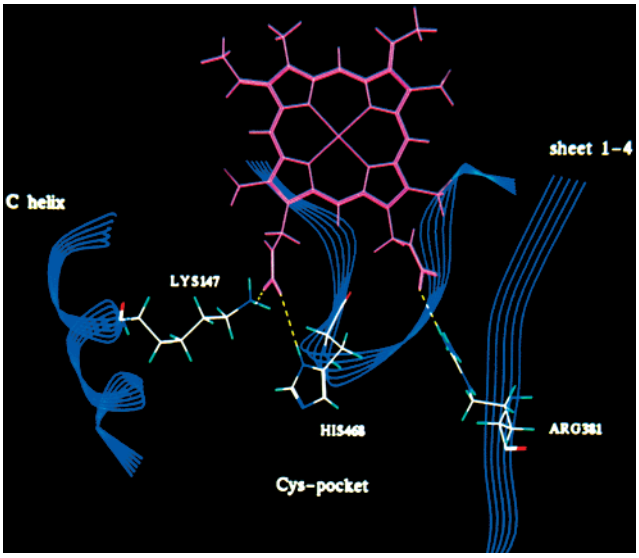

Figure 5. Stereoview of the conserved residues involved in heme binding. The hydrogen bonds are indicated with dotted lines.

to allow for oxygen and water binding, which resulted in the hydrophilic center and the hydrophobic N-terminus and C-terminus of the helix I.

Heme Environment. As in the crystal structures, the heme in $P450_{14DM}$ model was bracketed between the proximal helix L and distal helix I. C470 provided the axial thiolate ligand for the heme iron atom (in Figure 5). The side chain of the invariant phenylanine F463 completed the hydrophobic enclosure for the cysteine in combination with other highly conserved residues such as I471 and A476. The Cys-pocket appeared to serve an important role for establishing the redox potential of the heme iron, as observed in fluconazole-resistant mutation isolates G464S[53] and R467K.[54] Further, propionate coordination had been suggested to have an influence on the redox potential of the heme iron and was accomplished by three conserved basic residues in the $P450_{14DM}$. K147 at the N-terminal end of the helix C formed a salt bridge to the D-ring propionate, while R468 in the Cys-pocket formed an H-bond with D-ring propionate. R381 in β1-4 formed another salt bridge with A-ring propionate.

Redox-Partner Interaction and Electron Transfer. All the P450s must receive electrons from a reductase. In the case of microsomal P450s, the reductase was NADPH-cytochrome P450 reductase or cytochrome *b*5. A considerable amount of experimental evidence suggested that P450s interacted with their electron donor at the proximal surface of the molecule by forming an electrostatic complex. The electron donor was expected to be the acidic partner donating negative charges. P450s were the positively charged partner. Regions on the proximal surface of the $P450_{14DM}$ model that appeared to be involved in redox-partner binding were those in helices C, J, J′, K, and K″, and β1-3, β1-4, β2, β5, Meander, and Cys-pocket, which formed a concave depression in the proximal surface. Among them, the highly conserved basic residues such as K143 and K147 at the N-terminal end of the helix C, K398 between β2-2 and β1-3, and R467 and H468 in the Cys-pocket were the identical and/or very similar binding sites for electron donor on various P450s (in Figure 6). The residues unique to $P450_{14DM}$ such as K99 and H101 in helix B, K358 in helix J′, and R426, K433, K451, and K454 in the Meander and Cys-pocket were also the potential candidates for participating in reductase recognition. In addition, F463 and H468 probably played an essential role in the electron transfer.

Substrate Access Channel. The substrate binding pocket was embelled in the interior of the P450 proteins. The active site heme was accessible through a long channel. It was believed from the crystal structures that the hydrophobic substrate was recognized on the surface

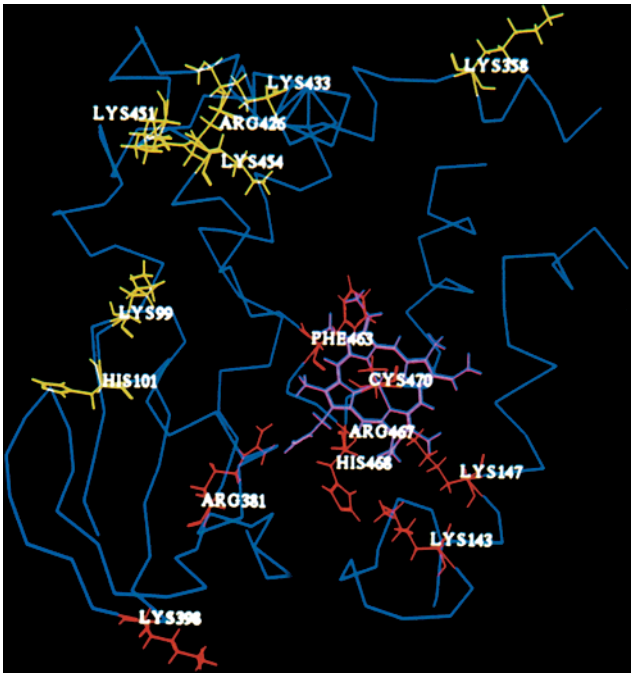

Figure 6. Proximal faces of the modeled structure. The residues probably interacted with redox-partner and/or involved in electron transfer were indicated.

Table 1. Active Site Residues of $P450_{14DM}$ of *C. albicans* within 8 Å from the Substrate

motifs	position in sequence	residues
β1-5−B′ loop	114−119	AEDAYK
B′ helix	120−130	HLTTPVFGKGV
Meander1	131−137	IYDCPNS
F helix C-terminus	220−231	LYSDLDKGFTPI
I helix	295−317	QEIANLLIGILMGGQHTSASTSA
β6-1 sheet	374−381	MPLHSIFR
β6-2 sheet	507−512	SMVVLP

of the protein by a hydrophobic patch of amino acid residues adjacent to the substrate access channel. In $P450_{14DM}$, this would correspond to residues L88, I91, and M92 in the β1-2, and L238 and L240 at the N-terminal end of helix G. It acted as the flexible flap or lid over the substrate access channel. The substrate then entered the mouth of the access channel and partitioned down into the active site as a result of hydrophobic interactions. The hydrophobic and aromatic residues lining the substrate access channel included F71 and F72 in helix A; F83, F85, and L87 in β1-1; L224 at the C-terminal of helix F; F228, I231, F233, V234, and F235 in the F−G loop; and M508 and V509 in β6−1.

Active Site of $P450_{14DM}$ and Substrate Binding. As in other P450s, the active site of $P450_{14DM}$ was bound at the bottom by the heme, and on the side by helix I, Meander1, β6-1/β1-4, and β6-2. Further outward from heme were the C-terminus of helix F and the β1-5−N-terminus of helix B′. The active site residues defined as those within 8 Å of any atom of substrate 24(28)-methylene-24,25-dihydrolanosterol are indicated in Table 1. Several amino acid residues, for example G303, H310, and S314, in helix I had been identified as substrate contact residues.[55,56] Helix I, Meander1, β6-1/β1-4, and β6-2 were SCRs and played an important role in catalysis reaction and substrate specificity. The C-terminus of helix F and the β1-5−N-terminus of helix B′ were spatially variable regions (SVRs). They composed the dome of the active site pocket and determined the size of the active site.

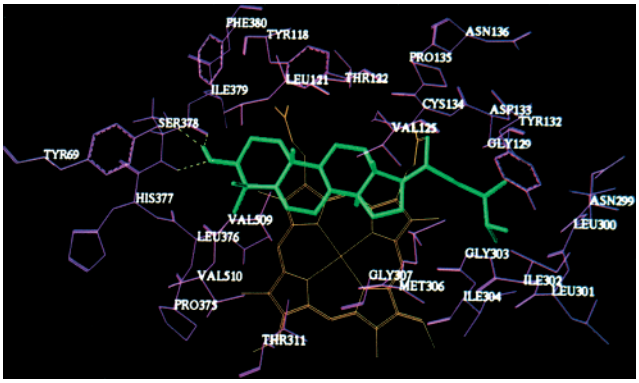

Figure 7. 24(28)-Methylene-24,25-dihydrolanosterol docked into the active site of lanosterol 14α-demethylase of *C. albicans*. The residues shown are within 4 Å from the substrate. The hydrogen bonds are indicated with dotted lines.

Figure 7 is the docking model of substrate into the active site of $P450_{14DM}$ from *C. albicans*, showing the residues within 4 Å from the substrate. The substrate was stabilized in the active site predominantly by hydrophobic interaction and hydrogen-bond binding. The distance from the iron atom to C32 of substrate, the oxidative site, was 5.066 Å. The 17-side chain of the substrate was deep in a narrow and highly hydrophobic cleft. The top of the binding cleft was formed by V125, G129, and Y132 of Meander1 and L301 of helix I, whereas C134, L300, I304 formed the bottom of the cleft. The side of this hydrophobic cleft was composed of residues P135, L301, G303, and M306. 24(28)-Methylene groups were in the favorable position of being parallel with the aromatic side chain of Y132 with a separation of 4 Å. The angular methyl group C18 of substrate formed close van der Waals interactions with the hydrophobic residues L121 and V509. The side chain methyl groups of V125 and T122 also made good van der Waals interactions with C19 of the substrate. In addition, V509 played an important role in the complementary fit between the valine side chain and the gem dimethyl groups C4β and C4α. Three hydrogen bonds were formed between the 3-OH group of substrate and carbonyl and amino groups of the main chain and hydroxyl group of the side chain of S378, which was essential for orienting the substrate to the correct direction in the active site. All the above analysis was in good agreement with lines of evidence suggesting that the 3-hydroxy group,[57] the angular methyl of the β-surface,[58] and the 17-side chain[59,60] of the substrate were the essential structures of substrate for interacting with the fungal $P450_{14DM}$ protein. These findings added further validity to the model. T311 was the highly conserved residues participating in the catalysis reaction of the substrate.

Modeling of Azole Antifungals in the Active Site of $P450_{14DM}$. Results of conformation sampling by the constrained systematic search method were indicated in Table 2. The results of the distance map in Figure 3 showed the acceptable distance range between pharmacophores. The pharmacophoric conformations of 14 azole antifungals matching the pharmacophore hypoth-

Table 2. Conformations in the Systematic Search

no.	systematic search	systematic search distance map	after filter	no.	systematic search distance constraints
14	2690	2690	539	**1**	188133
9	11269	2467	1089	**3**	184
12	30427	10603	10038	**4**	200
13	48856	18506	16587	**5**	6323
7	67291	9673	8029	**6**	6070
11	74792	4620	3036		
8	105293	5931	5931		
10	108159	8469	8469		

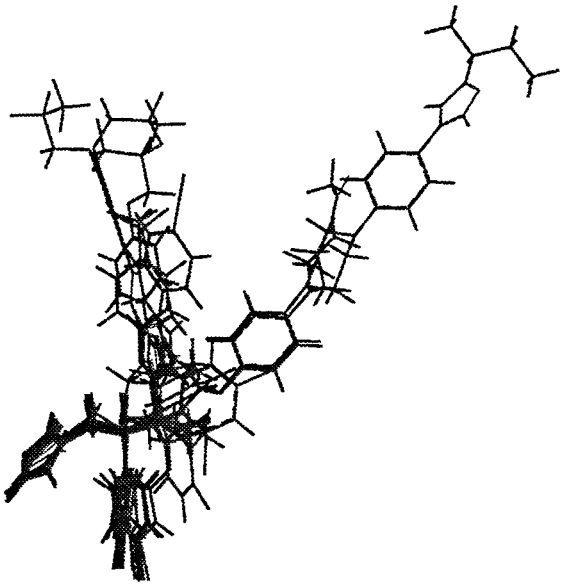

Figure 8. Stereorepresentation of 14 azole antifungals superimposed in pharmacophoric conformations.

Table 3. Energy Differences (ΔE) between the Active Conformer Energy (E_2) and the Global Minimum Energy (E_1)

no.	E_1	E_2	ΔE	no.	E_1	E_2	ΔE
1	18.824	22.516	3.692	**8**	26.387	26.400	0.013
2	20.250	20.838	0.588	**9**	126.255	127.946	1.191
3	26.562	33.660	7.098	**10**	34.910	37.676	2.766
4	40.760	44.124	3.364	**11**	18.130	18.324	0.194
5	40.677	41.541	0.864	**12**	15.879	15.879	0
6	45.347	47.722	2.365	**13**	20.167	21.901	1.734
7	40.803	40.875	0.072	**14**	28.009	29.151	1.142

esis were superimposed on the basis of the pharmacophores and shown in Figure 8. The good geometrical fit of the pharmacophores and the values of the energy difference between the resulting bioactive conformation and the global minimum energy conformation argued for a reasonable common conformation framework (in Table 3).

All 14 azole antifungals were shown to have a similar docking mode in the active site. The active site residues interacting with the inhibitors were the same as those interacting with the substrate, consisting of helix I, Meander1, and β6-1, which composed the side of the active site, and β6-2, C-terminus of helix F, and β1-5−N-terminus of helix B′, which made up of the dome of the active site. The docking modes of fluconazole and itraconazole into the active site of P45014DM from *C. albicans* were shown in parts A and B of Figure 9, respectively. The halogenated phenyl group of the inhibitors was located in the same hydrophobic binding cleft lined with V125, G129, Y132, C134, P135, L300, G303, I304, M306, and G307 as the 17-alkyl chain of

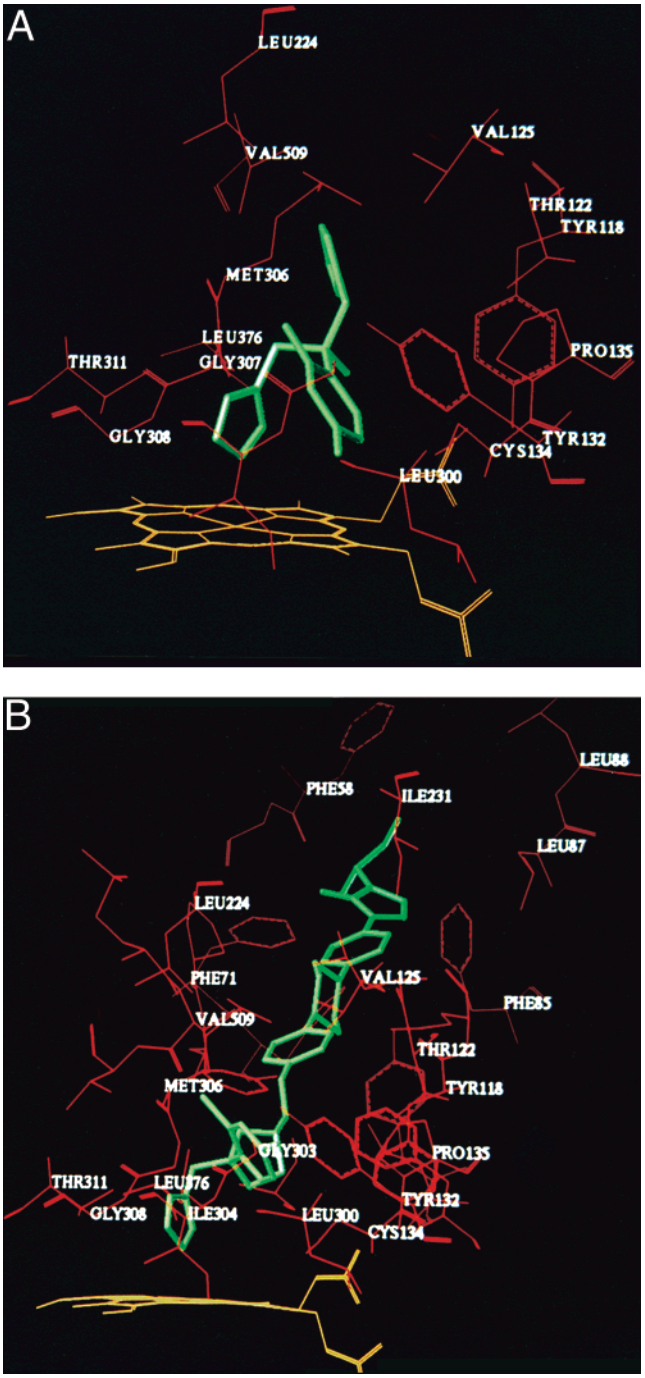

Figure 9. Stereoview of active site of lanosterol 14α-demethylase of *C. albicans* with bound fluconazole (A) and itraconazole (B).

substrate. Since the hydrophobic cleft was narrow, the space adjacent to positions 2 and 6 of the phenyl group was limited. The bulky substituents larger than a chlorine atom would probably produce significant steric clashes with residues C134 and G307, altering the docked ligand conformation substantially and lowering the binding affinity, such as in compounds **1**, **2**, and **3** in Table 4.[54] In contrast, the space adjacent to position 4 of the phenyl group was large enough to accommodate another phenyl ring, such as in compounds **6**, **7** in Table 4.[61] The binding energies ($E_{binding}$) of each inhibitor in Table 4 were calculated according to the formula

$$E_{binding} = E_{complex} - (E_{ligand} + E_{receptor})$$

Table 4. Chemical Structure, Antifungal Activities, and Binding Energies of Triazole Alcohols Interacting with the Active Site of $P450_{14DM}$ from *C. albicans*

Compd	IC_{50}(μM)[a]	E_{steric}(Kcal/mol)[b]	E_{elec}(Kcal/mol)[c]	E_{total}(Kcal/mol)[d]
1. 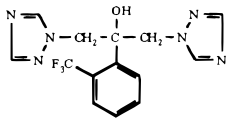	103.45	8.764	-47.548	-38.784
2. 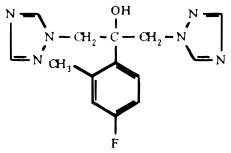	100.88	1.349	-50.036	-48.687
3. 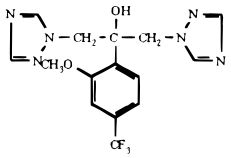	28.50	10.358	-43.474	-33.116
4. 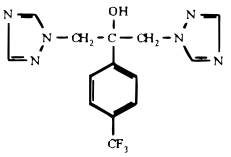	3.25	-14.850	-48.104	-62.954
5. 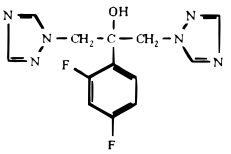	1.97	-16.312	-53.160	-69.328
6. 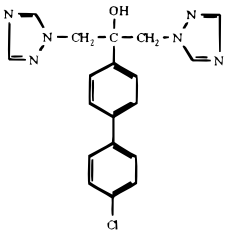	7.19	-16.312	-48.650	-64.963
7. 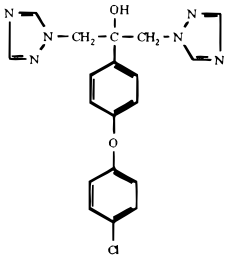	6.94	-16.147	-53.627	-69.774

[a] IC_{50} is the concentration required to reduce the growth of *C. albicans* to 50% of that in the control. [b] E_{steric} is the steric interaction energy. [c] E_{elec} is the electrostatic energy. [d] E_{total} is the total binding energy.

where E_{ligand} is the energy of the ligand corresponding to the overall minimum energy for the conformation search. $E_{receptor}$ is the energy of the receptor.

The halogenated phenyl ring of the inhibitors bound in close proximity to the flat aromatic ring of Y132, and a $\pi-\pi$ stacking interaction might exist between them. Replacement of Y132 has been found in the CYP51 protein of a fluconazole-resistant isolate of *C. albicans*, suggesting a critical role for this residue in the fluconazole susceptibility of CYP51.[62]

Although the side chains of itraconazole, ketoconazole, TAK-187, and D-0870 were very long, while the side chains of fluconazole, SM8668, and SDZ-89485 were rather short, all of them showed high antifungal activities. The reason was that all of them were of the pharmacophores proposed above and the spatial orien-

A

	β1-5—B′	Meander1	F	I	β6-1	β6-2
	118 126	129 136	224 231	300 312	375 380	507 511
CYP51(c.alb.)	YKHLTTPVF	GVIYDCPN	LDKGFTPI	LLIGILMGGQHTSA	PLHSIF	SMVVL
CYP51(c.tro.)	YTHLTTPVF	GVIYDCPN	LDKGFTPI	LLIGVLMGGQHTSA	PLHSIF	SMVTL
CYP51(s.cer.)	YAHLTTPVF	GVIYDCPN	LDKGFTPI	LLIGVLMGGQHTSA	PLHSLF	SMVTL
CYP51(s.pom.)	YSHLTTPVF	DVVYDIPN	LDQGFSPV	MMIALLMAGQHTSA	PIHSHM	SMVAL
CYP51(p.ita.)	YGKLTTPVF	DVVYDCPN	LDLGFSPI	MMITLLMAGQHSSS	SIHTLM	SLFSR
CYP51(human)	YSRLTTPVF	GVAYDVPN	LDGGFSHA	MLIGLLLAGQHTSS	PIMIMM	TMIHT
CYP51(rat)	YGRLTTPVF	GVAYDVPN	LDGGFSHA	MLIGLLLAGQHTSS	PIMTMM	TMIHT
CYP51(t.aes.)	Y-RFNVPTF	GVVFDVDY	LDNGMLPI	LLIAALFAGQHTSS	PLIMLL	AMVV-

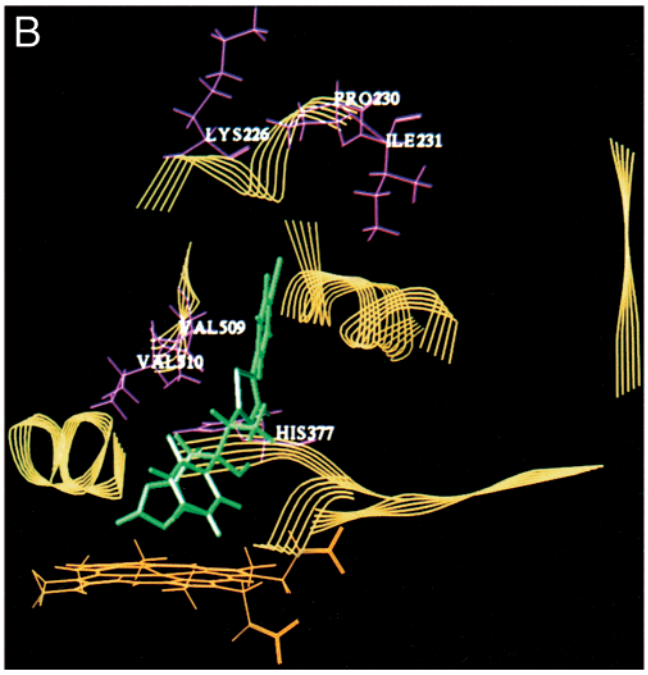

Figure 10. (A) Multiple sequence alignment of CYP51 proteins from *C. albicans* (c. alb.), *Candida tropicalis* (c. tro.), *S. cerevisiae* (s. cer.), *Schizosaccharomyces pombe* (s. pom.), *Penicillium italicum* (p. ita.), rat, human, and *Triticum aestivum* (t. aes.). Secondary structure features are labeled. (B) Stereoview of structrually selective residues of the active site of lanosterol 14α-demethylase of *C. albicans* relative to mammals in complex with ER-30346.

tations of the pharmacophores were very similar. The side chains of inhibitors were not the determinants for activity. They played a role in adjusting the physicochemical properties of the whole molecule to avoid some dissatisfying side effects and/or improve their pharmacokinetic and pharmacodynamic behavior. The side chains of itraconazole, ketoconazole, TAK-187, and D-0870 were too long to be accommodated in the active site. From the docking model shown in Figure 9, we found that the long side chains of the inhibitors surpassed the active site and interacted with the residues in the substrate access channel. Especially for itraconazole, the terminal alkyl group of the side chain reached the entrance of the substrate access channel and interacted with the hydrophobic residues F71, F85, L87, L88, and I231. This docking mode provided additional support for the general features of the $P450_{14DM}$ model.

A pharmacophore model of azole antifungals was proposed recently, including the N1 atom of the azole ring, the phenyl ring attached to C2, and another aromatic ring of miconazole, shown in Figure 2.[63] The phenyl ring attached to C2, also identified as a pharmacophore by us, occupies the hydrophobic cavity in the active site. It is obvious, however, that the N4(3) atom of the azole ring is more suitable than the N1 atom as another pharmacophore, because the N4(3) of the azole ring is convalently bound to the heme. The compound would be deprived of activity if N4(3) is replaced by a carbon atom. It seems that another aromatic ring for miconazole is not a determinant for antifungal activity, because neither SDZ-89485 nor SM-8668 have this aromatic ring. Furthermore, not only the physicochemical properties of the ring but the distances between this aromatic ring and other pharmacophores are variable in different azole antifungals, as shown in Figure 2. The chirality at C2 and C3 is important to antifungal activity. The compounds in Figure 2 exhibit significantly higher activities than the other stereoisomers.[49,50] So a methyl group attached to C3 was selected as a pharmacophore. The oxygen atom attached to C2 has been suggested to be favorable to antifungal activity; for example, triazole alcohols such as fluconazole, voriconazole, SM-8668, and D-0870 are the representatives of the second-generation triazole antifungals. They con-

stitute a considerable portion of the most recent promising leads in antifungal chemotherapy. These agents are generally more potent, better tolerated, metabolically more stable than the first-generation products which have no hydroxy group at the C3 position.[61,64] Nevertheless, we cannot find any one of the residues directly interacting with the oxygen atom from the docking model because the active site is so large that there is some distance between the oxygen atom and the residues around it. We think that waters conserved in the active site might act as the spacer to bridge the oxygen atom and the residue, probably H310 in the active site.

Figure 10 shows the multiple sequence alignment of the active site residues within 6 Å from any atom of the inhibitors. To compare with the mammalian enzyme, structurally selective residues of the active site of fungal $P450_{14DM}$ were distributed in the C-terminus of helix F, β-sheets 6-1 and 6-2, especially K226, P230, I231, H377, V509, and V510 in $P450_{14DM}$ from *C. albicans*. The physicochemical properties of these residues should be considered in designing new antifungals to improve their selectivity to $P450_{14DM}$ of fungi.

When we were preparing the manuscript, a three-dimensional molecular model of $P450_{14DM}$ from *Saccharomyces cerevisiae* based on homology with P450BM3 was reported.[65] The sequence alignment was similar to that of ours, with only a few differences in the N-terminus of the protein. S378 was also identified to interact with the 3-hydroxy group of the substrate, and the 17-alkyl side chain was deep in the same hydrophobic cavity. F145 in helix C or Y132 in Meander1 was proposed to interact with the planar dimethyl alkene in the 17-alkyl side chain of lanosterol. In our model, however, only Y132 was able to interact with the planar unsaturated region in the side chain of the substrate. The halogenated phenyl ring of ketoconazole was also proposed to occupy the same hydrophobic cavity as the 17-alkyl side chain in their model. However, their model invoked a fairly dramatic movement of the residues in the active site when ketoconazole was docked into the active site, and F134 formed a $\pi-\pi$ stacking interaction with the halogenated phenyl ring. In our model, it was the aromatic ring of Y132 that formed the $\pi-\pi$ stacking interaction with the halogenated phenyl ring of ketoconazole, and residues in the active site did not move obviously.

Conclusions

A homologous 3D model of lanosterol 14α-demethylase from *C. albicans* was built on the basis of the crystal coordinates of four known prokaryotic P450s: P450BM3, P450cam, P450terp, and P450eryF. The reliability of the model was assessed by Ramachandran plots, Profile-3D, hydropathy plot analysis, and by analyzing the consistency of the model with the experimental data on the $P450_{14DM}$. The overall structure of the resulting $P450_{14DM}$ model is similar to those of the known crystal structures. The model retains the core structure characteristic for cytochrome P450s. Most of the insertions and deletions expose the molecular surface. The structurally and functionally important residues such as the heme binding residues, the residues interacting with the redox-partner protein and/or involved in electron transfer, the residues lining the substrate access channel, and the substrate and the inhibitor binding residues were identified from the model. These analyses provide a basis for experiments to probe structure−function relationships in the $P450_{14DM}$. Exposed regions of the $P450_{14DM}$ have been identified which would be candidates for synthesis as peptides for the generation of polyclonal or monoclonal antibodies. Such isoenzyme-specific antibodies can be used to probe the P450 function by either blocking substrate binding or association of the enzyme with cytochrome P450 reductase. Mutagenesis of specific residues should establish whether they play a role in determining substrate and/or inhibitor specificity. Identification of such residues will allow the rational design of specific inhibitors and enzymes with altered substrate specificity.

Although one could not have the same degree of confidence in the model as in an experimentally determined structure, the careful building process and the results obtained from the experiments indicated that our model is reliable enough to be used for exploring the structure and function relationship. Preliminary work has been done on this issue, and promising results have been obtained, although further investigation is still needed in order to gain insight into the molecular mechanism of the interaction between $P450_{14DM}$ and its substrates and inhibitors. The next step in this line of research will be the design of lead inhibitors based on the active site and the extensive investigation of the structure and activity relationships. Finally, it should be pointed out that the robust strategy developed could serve as a guide to model other mammalian P450s and related system.

Acknowledgment. This work was supported in part by the National Natural Science Foundations of China (Grants No. 39770876, 39470830).

References

(1) Trzaskos, J. M.; Fischer, R. T.; Favata, M. F. Mechanistic studies of lanosterol C-32 demethylation conditions which promote oxysterol intermediate accumulation during the demethylation process. *J. Biol. Chem.* **1986**, *261*, 16937−16942.
(2) Aoyama, Y.; Yoshida, Y.; Sonoda, Y.; Sato, Y. Metabolism of 32-hydroxy-24,25-dihydrolanosterol by purified cytochrome P-45014DM from yeast. *J. Biol. Chem.* **1987**, *262*, 1239−1243.
(3) Aoyama, Y.; Yoshida, Y.; Sonoda, Y.; Sato, Y. Deformylation of 32-oxo-24,25-dihydrolanosterol by the purified cytochrome $P\text{-}450_{14DM}$ (Lanosterol 14α-demethylase) from yeast evidence confirming the intermediate step of lanosterol 14α-demethylation. *J. Biol. Chem.* **1989**, *264*, 18502−18505.
(4) Fischer, R. T.; Trzaskos, J. M.; Magolda, R. L.; Ko, S. S.; Brosz, C. S.; Larsen, B. Lanosterol 14α-methyl demethylase isolation and characterization of the third metabolically generated oxidative demethylation intermediate. *J. Biol. Chem.* **1991**, *266*, 6124−6132.
(5) Shyadehi, A. Z.; Lamb, D. C.; Kelly, S. L.; Kelly, D. E.; Schunck, W.-H.; Wright, J. N.; Corina, D.; Akhtar, M. The mechanism of the acyl-carbon bond cleavage reaction catalyzed by recombinant sterol 14α-demethylase of *Candida albicans*. *J. Biol. Chem.* **1996**, *271*, 12445−12450.
(6) Lamb, D. C.; Kelly, D. E.; Kelly, S. L. Molecular diversity of sterol 14α-demethylase substrates in plants, fungi and humans. *FEBS Lett.* **1998**, *425*, 263−265.
(7) Aoyama, Y.; Noshiro, M.; Gotoh, O.; Imaoka, S.; Funae, Y.; Kurosawa, N.; Horiuchi, T.; Yoshida, Y. Sterol 14α-demethylase P450 (P45014DM) is one of the most ancient and conserved P450 species. *J. Biochem.* **1996**, *119*, 926−933.
(8) Yoshida, Y.; Noshiro, M.; Aoyama, Y.; Kawamoto, T.; Horiuchi, T.; Gotoh, O. Structural and evolutionary studies on sterol 14-demethylase P450 (CYP51), the most conserved P450 monooxygenase: II. Evolutionary analysis of protein and gene structures. *J. Biochem.* **1997**, *122*, 1122−1128.

(9) Lamb, D. C.; Kelly, D. E.; Venkateswarlu, K.; Manning, N. J.; Bligh, H. F.; Schunck, W. H.; Kelly, S. L. Generation of a complete, soluble, and catalytically active sterol 14α-demethylase-reductase complex. *Biochemistry* **1999**, *38*, 8733−8738.
(10) Cabello-Hurtado, F.; Taton, M.; Forthoffer, N.; Kahn, R.; Bak, S.; Rahier, A.; Werck-Reichhart, D. Optimized expression and catalytic properties of a wheat obtusifoliol 14α-demethylase (CYP51) expressed in yeast. Complementation of erg11Delta yeast mutants by plant CYP51. *Eur. J. Biochem.* **1999**, *262*, 435−446.
(11) Bellamine, A.; Mangla, A. T.; Nes, W. D.; Waterman, M. R. Characterization and catalytic properties of the sterol 14α-demethylase from *Mycobacterium tuberculosis*. *Proc. Natl. Acad. Sci U.S.A.* **1999**, *96*, 8937−8942.
(12) Lai, M. H.; Kirsh, D. R. Nucleotide sequence of cytochrome P450LIA1 (lanosterol 14α-demethylase) from *Candida albicans*. *Nucleic Acid Res.* **1989**, *17*, 804.
(13) Van Nistelrooy, J. G. M.; van der Brink, J. M.; van Kan, J. A. L.; van Gorcom, R. F. M.; de Waard, M. A. Isolation and molecular characterisation of the gene encoding eburicol 14α-demethylase (CYP51) from *Penicillium italicum*. *Mol. Gen. Genet.* **1996**, *250*, 725−733.
(14) Nitahara, Y.; Aoyama, Y.; Horiuchi, T.; Noshiro, M.; Yoshida, Y. Purification and characterization of rat sterol 14-demethylase P450(CYP51) expressed in *Escherichia coli*. *J. Biochem.* **1999**, *126*, 927−933.
(15) Stromstedt, M.; Rozman, D.; Waterman, M. R. The ubiquitously expressed human CYP51 encodes lanosterol 14α-demethylase, a cytochrome P450 whose expression is regulated by oxysterols. *Arch. Biochem. Biophys.* **1996**, *329*, 73−81.
(16) Poulos, T. L.; Finzel, B. C.; Howard, A. J. High-resolution crystal structure of cytochrome P450cam. *J. Mol. Biol.* **1987**, *195*, 687−700.
(17) Hasemann, C. A.; Ravichandran, K. G.; Peterson, J. A.; Deisenhofer J. Crystal structure and refinement of cytochrome P450terp at 2.3A resolution. *J. Mol. Biol.* **1994**, *236*, 1169−1185.
(18) Cupp-Vickery, J. R.; Poulos, T. L. Structure of cytochrome P450eryF involved in erythromycin biosynthesis. *Natl. Struct. Biol.* **1995**, *2*, 144−153.
(19) Ravichandran, K. G.; Boddupalli, S. S.; Hasemann, C. A.; Peterson, J. A.; Deisenhofer J. Crystal structure of hemoprotein domain of P450BM3, a prototype for microsomal P450's. *Science* **1993**, *261*, 731−736.
(20) Hasemann, C. A.; Kurumbail, R. G.; Boddupalli, S. S.; Peterson J. A.; Deisenhofer J. Structure and function of cytochromes P450: A comparative analysis of three crystal structures. *Structure* **1995**, *2*, 41−62.
(21) Ji, H.-T.; Zhang W.-N.; Zhou Y.-J.; Lü, J.-G.; Zhu J. Zhu J. Comparative studies on crystal structures of four members of cytochrome P450 superfamily. *Acta Biochim. Biophys. Sin.* **1998**, *30*, 419−426.
(22) Zvelebil, M. J. J. M.; Wolf, C. R.; Sternberg, M. J. E. A predicted three-dimensional structure of human cytochrome P450: Implications for substrate specificity. *Protein Eng.* **1991**, *4*, 271−282.
(23) Szklarz, G. D.; Ornstein, R. L.; Halpert, J. R. Application of 3-dimensional homology modeling of cytochrome P450 2B1 for interpretation of site-directed mutagenesis results. *J. Biomol. Struct. Dyn.* **1994**, *12*, 61−78.
(24) Lin, D.; Zhang L. H.; Chiao, E.; Miller, W. L. Modeling and mutagenesis of the active site of human P450c17. *Mol. Endocrinol.* **1994**, *8*, 392−402.
(25) Laughton, C. A.; Zvelebil, M. J. J. M.; Neidle S. A detailed molecular model for human aromatase. *J. Steroid Biochem. Mol. Biol.* **1993**, *44*, 4−6.
(26) Lewis, D. F. Homology modelling of human cytochromes P450 involved in xenobiotic metabolism and rationalization of substrate selectivity. *Exp. Toxicol. Pathol.* **1999**, *51*, 369−374.
(27) Lozano, J. J.; Lopez-de-Brinas E.; Centeno N. B.; Guigo R.; Sanz F. Three-dimensional modelling of human cytochrome P450 1A2 and its interaction with caffeine and MeIQ. *J. Comput.-Aid. Mol. Des.* **1997**, *11*, 395−408.
(28) Lewis, D. F.; Dickins, M.; Lake, B. G.; Eddershaw, P. J.; Tarbit, M. H.; Goldfarb, P. S. Molecular modelling of the human cytochrome P450 isoform CYP2A6 and investigations of CYP2A substrate selectivity. *Toxicology* **1999**, *133*, 1−33.
(29) Dai, R.; Pincus, M. R.; Friedman, F. K. Molecular modeling of cytochrome P450 2B1: Mode of membrane insertion and substrate specificity. *J. Protein Chem.* **1998**, *17*, 121−129.
(30) Lewis, D. F.; Lee-Robichaud, P. Molecular modelling of steroidogenic cytochromes P450 from families CYP11, CYP17, CYP19 and CYP21 based on the CYP102 crystal structure. *J. Steroid Biochem. Mol. Biol.* **1998**, *66*, 217−233.
(31) Ruan, K.-H.; Milfeld, K.; Kulmacz, R. J.; Wu, K. K. Comparison of the concstruction of a 3-D model for human thromboxane synthase using P450camand BM-3 as templates: implications for the substrate binding pocket. *Protein Eng.* **1994**, *7*, 1345−1351.
(32) Graham-Lorence, S.; Amarneh, B.; White, R. E.; Peterson J. A.; Simpson E. R. A three-dimensional model of aromatase cytochrome P450. *Protein Sci.* **1995**, *4*, 1065−1080.
(33) Wang, L. H.; Matijevic-Aleksic, N.; Hsu, P. Y.; Ruan, K. H.; Wu, K. K.; Kulmacz, R. J. Identification of thromboxane A2 synthase active site residues by molecular modeling-guided site-directed mutagenesis. *J. Biol. Chem.* **1996**, *271*, 19970−19975.
(34) Boscott, P. E., Grant, G. H. Modeling cytochrome P450 14α-demethylase (*Candida albicans*) from P450cam. *J. Mol. Graph.* **1994**, *12*, 185−92, 195.
(35) Tsukuda, T.; Shiratori, Y.; Watanabe, M.; Ontsuka, H.; Hattori, K.; Shirai, M.; Shimma, N. Modeling, synthesis and biological activity of novel antifungal agents (1). *Bioorg. Med. Chem. Lett.* **1998**, *8*, 1819−1824.
(36) Holtje, H.-D.; Fattorusso, C. Construction of a model of the *Candida albicans* lanosterol 14α-demethylase active site using the homology modelling technique. *Pharm. Acta Helv.* **1998**, *72*, 271−277.
(37) TRIPOS Associates, Inc., 1699S. Hanley Road, Suite 303, St. Louis, MO 63144.
(38) Molecular Simulation Inc. 9685 Scranton Road, San Diego, CA 92121-3752.
(39) Needlman, S. B.; Wunsch, C. D. A general method applicable to the search for similarities in the amino acid sequences of two proteins. *J. Mol. Biol.* **1970**, *48*, 443−453.
(40) Maxifield, F. R.; Scheraga, H. A. Status of empirical methods for the prediction of protein backbone topography. *Biochemistry* **1976**, *15*, 5138−5153.
(41) Kyte, J.; Doolittle, R. F. A simple method for displaying the hydropathic character of a protein. *J. Mol. Biol.* **1982**, *157*, 105−132.
(42) Claessens, M.; van Cutsem, E.; Lasters, I.; Wodak S. Modelling the polypeptide backbone with 'spare parts' from known protein structures. *Protein Eng.* **1989**, *2*, 335−345.
(43) Luthy, R.; Bowie, J. U.; Eisenberg, D. Assessment of protein models with three-dimensional profiles. *Nature* **1992**, *356*, 83−85.
(44) Paulsen, M. D.; Ornstein, R. L. A 175-psec molecular dynamics simulation of camphor-bound cytochrome P-450_{cam}. *Proteins: Struct. Funct. Genet.* **1991**, *11*, 184−204.
(45) Plempel, M. Experience, recognitions and questions in azole antimycotics. *Shinkin to Shinkinsho* **1982**, *23*, 17−27.
(46) Yoshida, Y.; Aoyama, Y. Interaction of azole antifungal agents with cytochrome P-45014DM purified from *Saccharomyces cerevisiae* microsomes. *Biochem. Pharmacol.* **1987**, *36*, 229−235.
(47) Chuman, H.; Ito, A.; Saishoji, T.; Kumazawa S. QSARs and three-dimensional shape studies of fungicidal azolylmethylcyclopentanols. *ACS Symp. Ser.* **1995**, *606*, 171−185.
(48) Walker, K. A. M.; Hirschfeld, D. R.; Marx M. Antimycotic imidazoles. 2. Synthesis and antifungal properties of esters of 1-[2-hydroxy(mercapto)-2-phenylethyl]-1H-imidazoles. *J. Med. Chem.* **1978**, *21*, 1335−1338.
(49) Tasaka, A.; Kitazaki, T.; Tsuchimori, N.; Matsushita, Y.; Hayashi, R.; Okonogi, K.; Itoh, K. Optically active antifungal azoles. VII. Synthesis and antifungal activity of stereoisomers of 2-[(1R, 2R)-2-(2,4-difluorophenyl)-2-hydroxy-1-methyl-3-(1H-1,2,4-triazol-1-yl)propyl]-4-[4-(2,2,3,3-tetrafluoropropoxy)phenyl]-3(2H,4H)-1,2,4-triazolone (TAK-187). *Chem. Pharm. Bull.* **1997**, *45*, 321−326.
(50) Rotstein, D. M.; Kertesz, D. J.; Walker, K. A. M.; Swinney, D. C. Stereoisomers of Ketoconazole: Preparation and biological activity. *J. Med. Chem.* **1992**, *35*, 2818−2825.
(51) Tasaka, A.; Tamura, N.; Matsushita, Y.; Teranishi, K.; Hayashi, R.; Okonogi, K.; Itoh, K. Optically active antifungal azoles. I. synthesis and antifungal activity of (2R,3R)-2-(2,4-difluorophenyl)-3-mercapto-1-(1H- 1,2,4-triazol-1-yl)-2-butanol and its stereoisomers. *Chem. Pharm. Bull.* **1993**, *41*, 1035−1042.
(52) Raag, R.; Li, H.; Jones, B. C.; Poulos, T. L. Inhibitor-induced conformational change in cytochrome P-450_{CAM}. *Biochemistry* **1993**, *32*, 4571−4578.
(53) Kelly, S. L.; Lamb, D. C.; Loeffler, J.; Einsele, H.; Kelly, D. E. The G464S amino acid substitution in *Candida albicans* sterol 14α-demethylase causes fluconazole resistance in the clinic through reduced affinity. *Biochem. Biophys. Res. Commun.* **1999**, *262*, 174−179.
(54) White, T. C. The presence of an R467K amino acid substitution and loss of allelic variation correlate with an azole-resistant lanosterol 14α-demethylase in *Candida albicans*. *Antimicrob. Agents Chemother.* **1997**, *41*, 1488−1494.
(55) Ishida, N.; Aoyama, Y.; Hatanaka, R.; Oyama Y.; Imajo, S.; Ishiguro, M.; Oshima, T.; Nakazato, H.; Noguchi, T.; Maitra, U. S.; Mohan, V. P.; Sprinson, D. B.; Yoshida, Y. A single amino acid substitution converts cytochrome $P450_{14DM}$ to an inactive form, cytochrome $P450_{SG1}$: complete primary structures deduced from clone DNAs. *Biochem. Biophy. Res. Commun.* **1988**, *155*, 317−323.

(56) Lamb, D. C.; Kelly, D. E.; Schunck, W.-H.; Shyadehi, A. Z.; Akhtar, M.; Lowe, D. J.; Baldwin, B. C.; Kelly, S. L. The Mutation T315A in candida albicans sterol 14α-demethylase causes reduced enzyme activity and fluconazole resistance through reduced affinity. *J. Biol. Chem.* **1997**, *272*, 5682−5688.
(57) Aoyama, Y.; Yoshida, Y.; Sonoda, Y.; Sato, Y. The 3-hydroxy group of lanosterol is essential for orienting the substrate in the substrate site of cytochrome P-450_{14DM}. *Biochim. Biophys. Acta* **1989**, *1006*, 209−213.
(58) Aoyama, Y.; Yoshida, Y.; Sonoda, Y.; Sato Y. Role of the 8-double of lanosterol in the enzyme−substrate interaction of cytochrome P-450_{14DM}. *Biochim. Biophys. Acta* **1989**, *1001*, 196−200.
(59) Aoyama, Y.; Yoshida, Y.; Sonoda, Y.; Sato Y. Role of the side chain of lanosterol in substrate recognition and catalytic activity of lanosterol 14α-demethylase of yeast. *Biochim. Biophys. Acta* **1991**, *1081*, 262−266.
(60) Aoyama, Y.; Yoshida, Y.; Sonoda, Y.; Sato, Y. Structure analysis of the interaction between the side-chain of substrates and the active site of lanosterol 14α-demethylase of yeast. *Biochim. Biophys. Acta* **1992**, *1122*, 251−255.
(61) Klopman, G.; Ptchelintsev, D. Antifungal triazole alcohols: a comparative analysis of structure−activity, structure-teratogenicity and structure-therapeutic index relationships using the multiple computer-automated structure evaluation (Multi-CASE) methodology. *J. Comput.-Aided Mol. Des.* **1993**, *7*, 349−362.
(62) Asai, K.; Tsuchimori, N.; Okonogi, K.; Perfect, J. R.; Gotoh, O.; Yoshida, Y. Formation of azole-resistant *Candida albicans* by mutation of sterol 14-demethylase P450. *Antimicrob. Agents Chemother.* **1999**, *43*, 1163−1169.
(63) Talele, T. T.; Kulkarni V. M. Three-dimensional quantitative structure−activity relationship (QSAR) and receptor mapping of cytochrome P-$450_{14\alpha DM}$ inhibiting azole antifungal agents. *J. Chem. Inf. Comput. Sci.* **1999**, *39*, 204−210.
(64) Bartroli, J.; Turmo, E.; Alguero, M.; Boncompte, E.; Vericat, M. L.; Conte, L.; Ramis, J.; Merlos, M.; Garcia-Rafanell, J.; Forn, J. New azole antifungals. 2. Synthesis and antifungal activity of heterocyclecarboxamide derivatives of 3-amino-2-aryl-1-azolyl-2-butanol. *J. Med. Chem.* **1998**, *41*, 1855−1868.
(65) Lewis, D. F. V.; Wiseman, A.; Tarbit, M. H. Molecular modelling of lanosterol 14α-demethylase (CYP51) from *Saccharomyces cerevisiae* via homology with CYP102, a unique bacterial cytochrome P450 isoform: quantitative structure−activity relationships (QSARs) within two related series of antifungal azole derivatives. *J. Enzyme Inhibit.* **1999**, *14*, 175−192.

JM990589G